Human Thoracic and Abdominal Aortic Aneurysmal Tissues: Damage Experiments, Statistical Analysis and Constitutive Modeling

David M. Pierce[a], Franz Maier[b], Hannah Weisbecker[b], Christian Viertler[c], Peter Verbrugghe[d], Nele Famaey[e], Inge Fourneau[f], Paul Herijgers[d], Gerhard A. Holzapfel[b,*]

[a] *Departments of Mechanical Engineering, Biomedical Engineering and Mathematics, University of Connecticut, Connecticut, U.S.A.*

[b] *Institute of Biomechanics, Graz University of Technology, Graz, Austria*

[c] *Institute of Pathology, Medical University Graz, Graz, Austria*

[d] *Experimental Cardiac Surgery, Faculty of Medicine, UZ Leuven, Leuven, Belgium*

[e] *Department of Mechanical Engineering, KU Leuven, Leuven, Belgium*

[f] *Vascular Surgery, Faculty of Medicine, UZ Leuven, Leuven, Belgium*

Submitted to

Journal of the Mechanical Behavior of Biomedical Materials

June 4, 2014

*Corresponding author. E-mail: holzapfel@tugraz.at

Abstract Development of aortic aneurysms include significant morphological changes within the tissue: collagen content increases, elastin content reduces and smooth muscle cells degenerate. We seek to quantify the impact of these changes on the passive mechanical response of aneurysms in the supra-physiological loading range via mechanical testing and constitutive modeling. We perform uniaxial extension tests on circumferentially and axially oriented strips from five thoracic (65.6 years $\pm$ 13.4, mean $\pm$ SD) and eight abdominal (63.9 years $\pm$ 11.4) aortic fusiform aneurysms to investigate both continuous and discontinuous softening during supra-physiological loading. We determine the significance of the differences between the fitted model parameters: diseased thoracic versus abdominal tissues, and healthy (*J. Mech. Behav. Biomed. Mater.* **12**:93–106, 2012) versus diseased tissues. We also test correlations among these parameters and age, Body Mass Index (BMI) and preoperative aneurysm diameter, and investigate histological cuts. Tissue response is anisotropic for all tests and the anisotropic pseudo-elastic damage model fits the data well for both primary loading and discontinuous softening which we interpret as damage. We found statistically relevant differences between model parameters fitted to diseased thoracic versus abdominal tissues, as well as between those fitted to healthy versus diseased tissues. Only BMI correlated with fitted model parameters in abdominal aortic aneurysmal tissues.

Keywords human aorta, aortic aneurysm, supra-physiological loading, constitutive modeling, damage modeling

1. Introduction

Cardiovascular diseases, one of the leading causes of death in the Western world, account for 40% of the deaths in the European Union (Nichols et al., 2012). Among these diseases, aortic aneurysms stand out for their high mortality rate in cases of rupture; 85-95% for abdominal aortic aneurysms (AAA) (Kniemeyer et al., 2000). Aortic aneurysms are permanent dilations of the vessel exhibiting a diameter 50% larger than that in health, or for AAA specifically, a diameter larger than $3\,$cm (Shimizu et al., 2006). Currently the only treatment for an aortic aneurysm, which may grow and rupture, is elective surgical repair (Humphrey and Holzapfel, 2012). Such surgical repairs are either open or endovascular (catheter-based) procedures, where the later generally reduces pain and hospitalization time for patients. Unfortunately, the surgeries themselves carry high risk and do not necessarily increase the survival rate (Lederle et al., 2002). Hence there is a great need to more accurately assess both AAA rupture risk and the risk of specific surgical procedures to aid decision making in the clinical setting.

Different clinical approaches do exist to estimate the rupture risk of aneurysms. Most mod-

ern hospitals use the diameter criterion which recommends aneurysm repair if the diameter exceeds 5-5.5 cm. Despite its rudimentary nature this criterion can be measured with standard devices, such as ultrasound, and the result is immediately available. Another often used criterion is the growth rate of the aneurysm diameter. To effectively measure the growth rate of an aneurysm it must be detected early such that time is available for monitoring and decision making. While both diameter and growth rate initially appear relative easy to measure, variations in imaging planes and the non-circular nature of most aneurysms can lead to significant variations in the results. To overcome these disadvantages Kitagawa et al. (2013) suggested to measure the volume of an aneurysm using precise 3-D imaging methods in conjunction with modern image segmenting software, but this has not yet been applied clinically. Martin et al. (2013) estimated the rupture potential of ascending thoracic aneurysms by calculating a failure diameter, the diameter when tension within the wall was higher than the ultimate tension, using the law of Laplace in combination with data from uniaxial mechanical tests. Despite gross simplifications, results compared well with those observed clinically. There is still significant room for improvement of rupture-risk prediction methods for aneurysms, see, e.g., Vorp (2007) or Humphrey and Holzapfel (2012), or Raut et al. (2013) which describes the influence of geometric and biomechanical factors on risk estimations.

Clinical acquisition of patient-specific 3-D images opens the possibility to estimate more sophisticated rupture-risk predictors based on finite element (FE) analysis and tissue biomechanics. Accurate constitutive models for the tissue components are crucial in generating accurate simulation results. Biomechanicians generally model healthy arterial wall as an isotropic elastin matrix with reinforcing collagen fibers which are symmetrically-oriented and either well-aligned (Holzapfel et al., 2000) or dispersed Gasser et al. (2006) in orientation. Contrary to healthy aortic tissues, little experimental data on the stress-strain response of aneurysmal tissues currently exist for use in calibrating FE simulations of AAA tissues. Vande Geest et al. (2006) performed biaxial extension tests on AAA samples and clearly showed nonlinear, anisotropic responses which were stiffer in the circumferential direction. Tong et al. (2011) reported similar anisotropic responses for AAA wall tissues covered by intraluminal thrombus (ILT). Sokolis et al. (2012) performed uniaxial extension tests to failure on separated layers of ascending thoracic aortic aneurysms (TAAs) and also reported that the tissue was stiffer in the circumferential direction.

There are other constituents, beyond the vessel wall, present in aortic aneurysms, constituents which potentially impact the overall mechanical behavior. ILT often covers the inner vessel walls of AAAs and should be considered in accurate FE models of aneurysms. Tong et al.

(2011) also tested the three individual layers (luminal, medial and abluminal) of ILTs in biaxial extension and reported that the luminal layer showed an age-dependent mechanical response, starting as isotropic and turning anisotropic with age, in contrast the medial and abluminal layers which were always isotropic. In a subsequent work Tong et al. (2014) quantified changes in the dissection energy of ILT with age, considering four stages of development, and connected these data to structural remodeling the tissue. Plaques – containing lipids, fibro-fatty composites and calcifications – constitute another structural element within vessel walls (Wu et al., 2013). Chai et al. (2013) performed indentation tests on plaque samples with low calcium content and showed a large variation in the stiffness within individual plaques. Mulvihill et al. (2013) further demonstrated that different plaques show significant variations in mechanical response and they identified voids within the plaques which increased the vulnerability of the whole structure.

In light of the potential for supra-physiological loading, researchers have extended constitutive models for vascular tissues to include effects from damage, capturing both continuous and discontinuous softening. In continuous theory softening (damage) accumulates throughout the entire load history while in discontinuous theory damage accumulates only when the applied loads exceed the previous maximum in the loading history. Balzani et al. (2006) introduced a model for discontinuous damage in the collagen fibers of the tissue and subsequently calibrated it successfully using one experimental data set from a human carotid artery (Balzani et al., 2012). Rodríguez et al. (2006) proposed another approach where collagen fibers were modeled as worm-like chains, and where the discontinuous softening was realized by considering individual strain energies for individual collagen fiber bundles and a beta-distribution of the rupture strain until fracture. Subsequently, Rodríguez et al. (2008) implemented this approach in an FE code to estimate the rupture risk of AAA tissues. Peña et al. (2009) developed a damage model for arterial tissues that accounts for both continuous and discontinuous softening, and that considers different damage evolutions for the matrix and two distinct fiber families. Using a complex experimental plan to determine the necessary parameters the authors fit both the preconditioning behavior and the Mullins's type softening of arterial tissues accurately. Gasser (2011) developed a microfiber model to describe the failure of collagen fibers due to irreversible rearrangements and loss of proteoglycan bridges which cause softening during supra-physiological loading.. Using material parameters estimated from the macroscopic mechanical tests, the model captures preconditioning of the tissue as well as both the low and high-strain regions of the tissue's stress-strain response. Rickaby and Scott (2013) modified a transversely-isotropic eight-chain model by adding softening functions for the primary loading path, the unloading and reloading paths. The authors fitted longitudinal and circumferential data

from a human thoracic aorta with excellent accordance, but unfortunately the model uses numerous parameters with unclear physical meanings. Recently, Schmidt et al. (2014) proposed a statistical approach to describe microscopic damage evolution in soft collagenous tissues. Within that model the statistical distributions of proteoglycan orientation, fibril length parameters and ultimate proteoglycan stretch were also considered. The applicability of the model approach within a FE framework was shown by simulating the overexpansion of simplified atherosclerotic arteries.

Efforts have been made to study specific surgical procedures which may generate high stresses and damage in the vasculature. Researchers have applied FE simulations to study specific medical applications, e.g., balloon-angioplasty (Balzani et al., 2006), stent interactions with vasculature (Mortier et al., 2010) and arterial clamping (Famaey et al., 2012). Vande Geest et al. (2008) applied FE analysis to estimate rupture-risk of patient's AAAs using only the estimated maximum principal stresses in the aneurysm wall. The authors tested simulations including either isotropic or anisotropic material models and while neither was able to significantly discriminate ruptured versus non-ruptured AAAs, the authors suggest, based on statistical analysis, that anisotropic models of patient-specific AAAs may help better identify AAAs at high risk. Badel et al. (2014) calculated the dissection risk of a coronary artery during the early stages of balloon angioplasty using FE analysis which considered the presence of a fibrous plaque and the medial layer imbedded in myocardium and epicardium. These simulations, using cohesive interfaces to model damage, showed a high risk of plaque detachment at the shoulder region of the plaque (in accordance with clinical findings) and a second risk zone within the arterial media where damage initiated at a very early stage of the procedure. Iannaccone et al. (2014) simulated, using the damage model of Balzani et al. (2006), the influence of lumen geometry, plaque morphology and composition on damage initiation and lumen gain during balloon angioplasty. The authors showed that eccentricity of the plaque causes high stresses in uncovered areas, stress which could lead to an increased failure rate during the procedure. Balakhovsky et al. (2014) estimated the damage evolution and failure risk in growing aneurysms using an approach developed by Volokh and Vorp (2008). The authors calculated the rupture potential of two basic geometries, one representing saccular aneurysms and the other fusiform aneurysms, with different initial fiber properties and found a range of parameters that lead to aneurysm rupture. While they reach qualitative agreement with clinical observations, they have not validated their estimations with model geometries and mechanical properties derived from human aneurysmal tissues. Romo et al. (2014) determined regions of higher rupture risk by calculating the stress distributions and thickness evolution of the vessel wall during inflation tests on ascending TAA

tissues. Contrary to the generally accepted theory that the tissues rupture at the location of the highest stress the authors claimed that locations of greatest reduction in thickness are most likely to fail.

The development and growth of an aortic aneurysm include significant morphological changes within the vessel wall – collagen content increases, elastin content reduces and smooth muscle cells degenerate (see, e.g., Tsamis et al. 2013) – and little experimental data exist for the stress-strain response of aortic aneurysms in the supra-physiological loading range. In this study we seek to quantify the impact of these changes on the passive mechanical response of diseased aortic tissues by estimating appropriate material parameters via mechanical testing and constitutive modeling. In our previous work, we modeled the supra-physiological stress-stretch response of the healthy thoracic and abdominal aortic tissues with an anisotropic pseudo-elastic damage model (Weisbecker et al., 2012). To facilitate direct comparison we assume that this model is also valid for diseased, i.e., remodeled, tissues. To this end we perform uniaxial extension tests on circumferentially and axially oriented strips from six thoracic and eight abdominal aortic fusiform aneurysms. By repeating three loading cycles per loading level we investigate both continuous and discontinuous softening. We fit the resulting data with our previous pseudo-elastic constitutive model to quantify damage that accumulates in the aortic tissue causing softening. We use the Wilcoxon rank sum test to determine the significance of differences between the fitted material parameters: diseased thoracic versus abdominal tissues, and healthy (from previous) versus diseased tissues. We also test correlations of our parameters with age, Body Mass Index (BMI) and preoperative aneurysm diameter. To gather additional information to interpret model parameters, we investigate histological cuts following standard procedures.

2. Materials and Methods

2.1. Constitutive model for arterial tissue including damage

Following Weisbecker et al. (2012) to model the material response of aortic tissues during supra-physiological loading, and to facilitate comparison between healthy and diseased tissues, we postulate a decoupled representation of a strain-energy function Ψ and use a similarly decomposed pseudo-elastic damage model as (Ogden and Roxburgh, 1999)

$$\Psi(J, \overline{\mathbf{C}}, \eta_{\mathrm{f},i}) = \Psi_{\mathrm{vol}}(J) + \overline{\Psi}^{0}_{\mathrm{m}}(\overline{\mathbf{C}}) + \sum_{i=4,6} [\eta_{\mathrm{f},i} \overline{\Psi}^{0}_{\mathrm{f},i}(\overline{\mathbf{C}}) + \Phi_{\mathrm{f},i}(\eta_{\mathrm{f},i})], \qquad i = 4, 6, \tag{1}$$

where here, and in all that follows, the index $i = 4, 6$ does not employ Einstein summation notation, instead it refers to a specific family of collagen fibers, Ψ_{vol} is a strictly convex function

which describes the volumetric elastic response, $\overline{\Psi}^0_{\mathrm{m}}$ describes the isochoric strain energy of the undamaged matrix material (the superscript 0 denotes an undamaged material), $\overline{\Psi}^0_{\mathrm{f},i}$ describes the isochoric strain energy of the undamaged fiber families, and $\Phi_{\mathrm{f},i}$ denote (smooth) damage functions of the two fiber families (NB. damage only accumulates in the deviatoric part of the strain-energy function and the material remains isochoric even under induced damage). Furthermore, $J = \det\mathbf{F} > 0$ is the determinant of the deformation gradient $\mathbf{F}$, $\overline{\mathbf{C}} = \overline{\mathbf{F}}^{\mathrm{T}}\overline{\mathbf{F}}$ is the modified right Cauchy-Green tensor with $\overline{\mathbf{F}} = (J^{-1/3}\mathbf{I})\mathbf{F}$ (Holzapfel et al., 2000), and $\eta_{\mathrm{f},i} \in]0,1]$ denote damage variables of the two fiber families defined as (Weisbecker et al., 2012)

$$\eta_{\mathrm{f},i} = 1 - \frac{1}{r_{\mathrm{f}}}\mathrm{erf}\left[\frac{1}{m_{\mathrm{f}}}(\overline{\Psi}^{\max}_{\mathrm{f},i} - \overline{\Psi}^0_{\mathrm{f},i})\right], \tag{2}$$

where $\overline{\Psi}^{\max}_{\mathrm{f},i}$ denote the maximum strain energies obtained in the fiber families over the deformation history, $r_{\mathrm{f}} > 1$ characterizes the maximum damage that can be induced in a fiber family under loading, and $m_{\mathrm{f}} > 0$ determines how fast softening accumulates in a fiber family (NB. we assume that damage evolves similarly in both fiber families so that damage can be fully described by the two parameters r_{f} and m_{f}). Small values of m_{f} indicate that significant damage occurs at relatively small strains, whereas larger values of m_{f} indicate damage will progress more slowly. We characterize damage induced in the fiber families by the minimum of the damage variables as

$$\eta^{\min}_{\mathrm{f},i} = 1 - \frac{1}{r_{\mathrm{f}}}\mathrm{erf}\left(\frac{1}{m_{\mathrm{f}}}\overline{\Psi}^{\max}_{\mathrm{f},i}\right). \tag{3}$$

Following Holzapfel et al. (2000) and Gasser et al. (2006) we model the arterial wall as a composite of matrix elastin with two dispersed, reinforcing collagen fiber families. We assume the non-collagenous matrix is isotropic and model it using the neo-Hookean strain-energy function

$$\overline{\Psi}^0_{\mathrm{m}} = \frac{\mu}{2}(\bar{I}_1 - 3), \tag{4}$$

where $\bar{I}_1 = \mathrm{tr}\overline{\mathbf{C}}$ is the first invariant of $\overline{\mathbf{C}}$ and $\mu > 0$ corresponds to the shear modulus of the material in the reference configuration. Based on experimental justification from Schriefl et al. (2012b) we assume two reinforcing collagen fiber families and model them using the anisotropic strain-energy functions

$$\overline{\Psi}^0_{\mathrm{f},i} = \frac{k_1}{2k_2}[e^{k_2(\bar{I}^\star_i - 1)^2} - 1], \qquad \bar{I}^\star_i = \kappa\bar{I}_1 + (1-3\kappa)\bar{I}_i, \tag{5}$$

where the pseudo-invariants $\bar{I}_4 = \overline{\mathbf{C}} : \mathbf{M}\otimes\mathbf{M}$ and $\bar{I}_6 = \overline{\mathbf{C}} : \mathbf{M}'\otimes\mathbf{M}'$ correspond to the squares of the stretches of the fibers in the fiber directions. The vectors $\mathbf{M}$ and $\mathbf{M}'$ denote the mean directions of the collagen fibers in the reference configuration. Since the fibers are

located in the tangential plane of the artery and symmetrically oriented with respect to the circumferential direction of the artery both $\mathbf{M}$ and $\mathbf{M}'$ are uniquely defined by the structural parameter φ, which defines the angle between the circumferential direction of the artery and the fiber directions; in the present study the parameter φ was used as a phenomenological (material) parameter. The dispersion parameter $\kappa \in [0, 1/3]$ describes the radial symmetry of dispersion of the fiber orientations about the mean fiber directions, k_1 is a stress-like parameter and k_2 is a dimensionless parameter. Herein the anisotropic strain-energy functions $(5)_1$ only contribute to Ψ when the fibers are extended (and not in compression), strictly when either $I_4 > 1$ and/or $I_6 > 1$. If one or more of these conditions is not satisfied then we omit the corresponding contributions of $(5)_1$.

With (1)-(5) we calculate the second Piola-Kirchhoff stress tensor as $\mathbf{S} = 2\partial\Psi/\partial\mathbf{C} = \mathbf{S}_{\text{vol}} + \overline{\mathbf{S}}$, where $\mathbf{S}_{\text{vol}} = 2\partial\Psi_{\text{vol}}/\partial\mathbf{C}$ and $\overline{\mathbf{S}}$ is the isochoric second Piola-Kirchhoff stress tensor which we calculate as

$$\overline{\mathbf{S}} = \overline{\mathbf{S}}^0_{\text{m}} + \sum_{i=4,6} \eta_{\text{f},i} \overline{\mathbf{S}}^0_{\text{f},i}, \qquad \overline{\mathbf{S}}^0_{\text{m}} = 2\frac{\partial \overline{\Psi}^0_{\text{m}}}{\partial \mathbf{C}}, \qquad \overline{\mathbf{S}}^0_{\text{f},i} = 2\frac{\partial \overline{\Psi}^0_{\text{f},i}}{\partial \mathbf{C}}, \tag{6}$$

where $\overline{\mathbf{S}}^0_{\text{m}}$ and $\overline{\mathbf{S}}^0_{\text{f},i}$ are isochoric second Piola-Kirchhoff stress tensors according to the primary loading curve. With a standard push-forward operation we obtain the Cauchy stress tensor $\boldsymbol{\sigma} = J^{-1}\mathbf{F}\mathbf{S}\mathbf{F}^{\text{T}}$. For a more detailed discussion of the constitutive model the reader is referred to Weisbecker et al. (2012) and references therein.

2.2. Experimental protocol

2.2.1. Sample preparation

We harvested 12 abdominal (69.7 years $\pm$ 4.4, mean $\pm$ SD) and seven thoracic (64.5 years $\pm$ 12.3)[1] tissue samples from true fusiform aortic aneurysms undergoing open surgical repair at Universitaire Ziekenhuizen (UZ) Leuven, Belgium. We stored all samples in physiological solution and froze them for transportation to Graz University of Technology, Austria, where they were stored at $-20°$C until experimental testing[2].

After unfreezing each sample, we carefully removed loose connective tissue attached to the adventitia so that only the wall itself remained for mechanical testing. With a punching tool

[1] Unfortunately we lost the data sheet (including sample-specific information) for one thoracic sample during transportation from Leuven, Belgium, to Graz, Austria, and thus we calculate the given mean value from the remaining six samples.

[2] The Ethical Committee of UZ Leuven approved the use of material from human subjects for the present study (approval number B32220071899).

we cutted out rectangular samples, measuring 4 mm in width and at least 15 mm in length, in both the axial and the circumferential directions of the tissue. We measured sample thickness with a videoextensiometer at four different points distributed evenly on each sample. To get a representative thickness for each sample we calculated the mean value of the four measurements. Finally, we stored the samples in physiological solution between preparation and testing to prevent dehydration.

In light of the available quality (some highly calcified) and size (some too small) of the samples, we were able to test thoracic tissues from six patients (denoted as T.1–T.6) and abdominal tissues from eight patients (A.1–A.8). To increase the amount of mechanical data we took more than one sample pair per patient (denoted with an additional index, e.g., A.8.1), if the size of the original tissue sample was sufficient. Table 1 shows the available patient-specific data for the patients where we list only five out of six total patients with TAAs because for one patient we had no data[1]. We provide additional information on the medical background and lifestyle of

Patient #	Gender M/F	Age years	Height cm	Weight kg	BMI -	Diameter mm
Thoracic aorta						
T.1	F	75	158	45	18.02	46
T.2	F	78	167	70	25.09	58
T.3	F	73	156	53	21.77	NA
T.4	M	51	173	83	27.73	48
T.5	M	51	186	98	28.32	49
Abdominal aorta						
A.1	M	73	175	85	27.75	73
A.2	M	59	178	73	23.04	59
A.3	M	60	162	83	31.62	60
A.4	M	70	176	88	28.40	70
A.5	F	60	169	75	26.20	60
A.6	F	52	165	87	31.95	52
A.7	M	52	174	75	24.77	52
A.8	M	85	166	70	25.40	85

Table 1: Patient-specific data: ‘M’ = male; ‘F’ = female; ‘BMI’ = Body Mass Index; ‘Diameter’ = patient’s preoperative aneurysm diameter; ‘NA’ = data not available.

the patients in Table A.4 of Appendix A.

2.2.2. Uniaxial tension test

We performed uniaxial mechanical tests on circumferentially and axially oriented strips from five thoracic (65.6 years $\pm$ 13.4, mean $\pm$ SD) and eight abdominal (63.9 years $\pm$ 11.4) aortic fusiform aneurysms. The tests were performed within a bath of physiological solution, kept at a constant temperature of 37°C, using a uniaxial testing machine. To ensure a secure connection to the testing device clamps and to prevent slippage we glued sandpaper to the ends of the samples. We also attached small rectangular foam markers to the samples in order to measure the displacement during testing using a videoextensiometer. Our testing procedure is force driven, where we calculated forces which result in the desired first Piola-Kirchhoff stresses of $25, 50, 75, 100, 200$ and 300 kPa. For each load step we performed three load cycles in order to observe both discontinuous softening (in the first loading cycle) and continuous softening (in the two following cycles to the same maximum load). To avoid dynamic or viscoelastic effects we performed testing under quasi-static conditions with a loading rate of 5 mm/min.

2.2.3. Data analysis and model fit

We completed all data analyses using a semi-automatic fitting procedure implemented in Matlab (R2011b, The MathWorks, Inc., Massachusetts, USA). To start, we preprocessed the force-displacement data sets to eliminate those data recorded either after rupture of the sample or when the sample slipped out of the testing clamps. In order to fit our constitutive damage model to the experimental data, we next calculated the stretch $\lambda = l/L$, where l is the deformed length of the sample (related to the displacement of the sample) and L is the reference length of the undeformed sample, both in the direction of loading. Subsequently we calculated the Cauchy stress σ as

$$\sigma = \frac{f}{TW}\lambda, \tag{7}$$

where f is the measured force, T is the initial thickness and W the initial width of the material, cf. Weisbecker et al. (2012). To reduce noise, we filtered the experimentally determined stretch and stress data with a Savitzky-Golay Filter of order two. We varied the frame size of the filter for each specimen (minimum of 41 data points to maximum of 151) depending on the noise but kept this as low as possible to avoid manipulating the data.

Given the experimentally determined stretch-stress data for each sample, we used the nonlinear least-square trust region algorithm implemented in Matlab to minimize the objective function

$$\chi = \sum_{i=1}^{n} [\sigma_i^{\mathrm{exp}} - \sigma_i^{\mathrm{mod}}(\mathbf{x}_j)]^2, \qquad j \in [\mathrm{mat}, \mathrm{dam}], \tag{8}$$

where n is the number of data points considered, $\sigma_i^{\exp}$ are the Cauchy stresses determined experimentally and σ_i^{mod} are the corresponding values predicted by our constitutive model including pseudo-elastic damage (1)-(6) for both axial and circumferential directions simultaneously, and $\mathbf{x}$ denotes a vector of model parameters (the subscript j denotes which of the parameters are fit with $j = \mathrm{mat}$ referring to material parameters and $j = \mathrm{dam}$ referring to damage parameters). To calculate the Cauchy stress response of the model we determined the lateral and the through-the-thickness stretches by invoking the incompressibility condition and an additional constraint that the stress in the lateral direction equals zero. Specifically, we first fitted the material parameters $\mathbf{x}_{\mathrm{mat}} = [\mu, k_1, k_2, \varphi, \kappa]$ to the primary loading curve. To improve the quality of our fit in the toe region of the loading curve, we performed an initial fit in this toe region separately to obtain the shear modulus μ which is largely responsible for the material behavior at low deformations. Next we obtained the damage parameters $\mathbf{x}_{\mathrm{dam}} = [r_{\mathrm{f}}, m_{\mathrm{f}}]$ by repeating the fitting procedure, i.e., by minimizing (8) using the fitted material parameters and the entire loading history. Note that we tested different sets of initial guesses for the model parameters as these may lead to different fitting results (Ogden et al., 2004), yet all physically-reasonable initial guesses resulted in nearly identical model parameters. We reported the complete set of fitted model parameters (material and damage) as well as the median values with their corresponding interquartile ranges, and provide the coefficient of determination R^2 to evaluate the goodness of fit.

2.2.4. Statistical analysis

We used statistical methods to determine if our fitted model parameters correlate significantly with a patient's age, BMI and preoperative aneurysm diameter using the rank correlation coefficient r_s. We also tested the significance of any correlations by calculating the confidence interval with the Fisher transformation. Due to the low number of thoracic samples we performed these calculations only for the abdominal aortic samples. Additionally, we used the Wilcoxon rank sum test to determine the significance of the differences among the fitted model parameters: those fitted to diseased thoracic versus abdominal tissues, and those fitted to healthy (from Weisbecker et al., 2012) versus diseased tissues. More specifically on the later, we compared the model parameters fitted to healthy *descending* thoracic tissue samples to those from diseased *ascending* thoracic samples because of the samples available. Here we adjusted the significance level with the Boferroni-Holm correction. For all tests we assumed $p < 0.05$ to be significant.

2.2.5. Histology

In close proximity to the areas of tissue cut out for mechanical testing, we also cut out additional samples and stored them in 4% buffered formaldehyde solution (pH 7.4) for histological investigations at the Medical University Graz, Austria. We performed histological studies on formalin fixed and parafin embedded cuts in the circumferential planes, normal to the axial directions of the samples. Following standard procedures we stained the samples with Hematoxylin and Eosin (H&E) to highlight cell cores, Picrosirius Red (PsR) to highlight fibrillar collagen and Elastica von Gieson (EvG) to highlight elastic fibers. We acquired images from a Nikon Eclipse 80i microscope (Nikon Corporation, Tokyo, Japan), set to either $20\times$ or $100\times$ magnification, using a Nikon Digital Sight DS-Fi1 digital camera.

3. Results

3.1. Material and damage parameters

We provide representative stress-stretch experimental data, model fits and corresponding evolutions of the damage variables in Fig. 1, where Figs. 1(a)-(b) correspond to the thoracic sample T.2.1 and Figs. 1(c)-(d) correspond to the abdominal sample A.8.2.

Both samples show (strongly) anisotropic mechanical behavior and significant hysteresis, representative for all samples tested. We provide the median values, interquartile ranges (Q_1 and Q_3, respectively) and coefficients of determination R^2 for material and damage parameters $\mu, k_1, k_2, \varphi, \kappa, r_{\mathrm{f}}$ and m_{f} fitted to the intact, human thoracic and abdominal aortic aneurysmal tissues in Table 2. The measured mean thickness is $2.12\,\mathrm{mm}\ \pm 0.43$ for the abdominal samples and $1.98\,\mathrm{mm}\ \pm 0.30$ for the thoracic samples.

3.2. Statistical analysis

The statistical analysis demonstrates no correlation among the fitted model parameters generated from intact AAA tissues and the patient's age or preoperative aneurysm diameter. Among all combinations tested, only BMI correlates in a statistically relevant manner with model parameters generated from AAA tissues, where both k_1 and κ increase with increasing BMI. For the parameter k_1 the rank correlation coefficient r_s equals 0.71 with a corresponding confidence interval CI of $[0.09, 0.93]$, while for the parameter κ, r_s and CI equals 0.78 and $[0.23, 0.95]$, respectively. We find statistically relevant differences (at $p < 0.05$) between diseased abdominal and thoracic samples for k_1 and κ, where both are higher in abdominal samples.

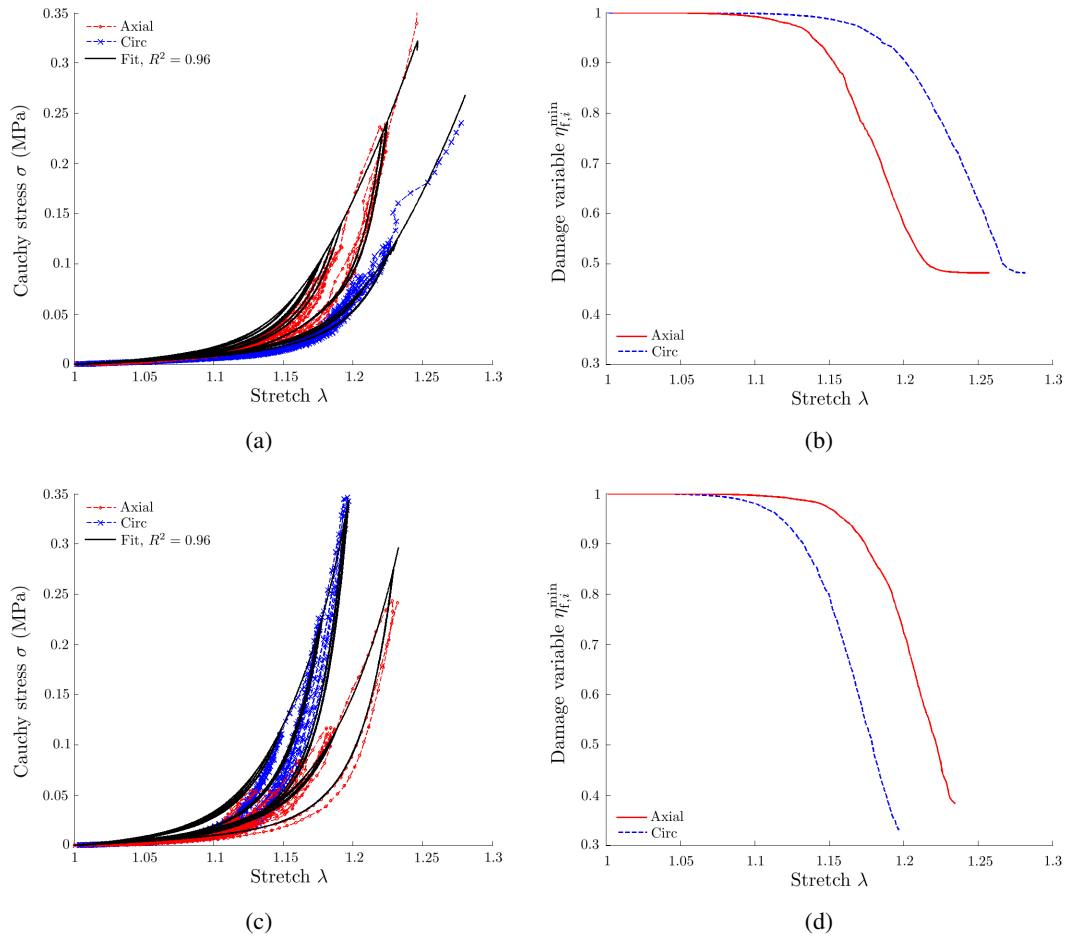

Figure 1: Representative stress-stretch experimental data, model fits and corresponding evolutions of the damage variables, where (a)-(b) correspond to the thoracic sample T.2.1 and (c)-(d) correspond to the abdominal sample A.8.2. Figures 2 and 3 provide corresponding histological images, respectively.

3.3. Comparison with healthy tissues

Table 3 reviews the material parameters for healthy intact (three-layer composite) tissues, see Weisbecker et al. (2012). When comparing intact aneurysmal tissues to healthy, intact (three-layer composite) tissues (Weisbecker et al., 2012) we find, for the human abdominal samples, statistically significant differences (at $p < 0.05$) for φ and the damage parameter m_{f}. We obtain a fiber angle close to $45°$ for AAA tissues. The damage variable, an indicator for strain dependency, is smaller for AAA tissues. For the human thoracic aneurysmal tissues, the model parameters μ and k_2 differ significantly from the corresponding parameters for healthy thoracic tissues. Here the shear modulus is higher, indicating a higher initial stiffness, while k_2 is smaller,

Patient	μ	k_1	k_2	φ	κ	r_f	m_f	R^2
#	[MPa]	[MPa]	[–]	[°]	[–]	[–]	[–]	[–]
Thoracic aortic aneurysm								
T.1.1	0.046	7.92	0.000	50.7	0.145	1.00	0.026	0.94
T.1.2	0.023	5.38	0.000	48.6	0.134	1.00	0.033	0.97
T.2.1	0.018	1.92	0.000	46.6	0.135	1.93	0.002	0.97
T.2.2	0.035	9.07	0.000	34.6	0.256	1.00	0.007	0.97
T.3.1	0.028	0.57	94.63	41.8	0.000	2.03	0.002	0.97
T.3.2	0.019	0.68	0.005	41.4	0.018	2.69	0.003	0.97
T.4.1	0.020	0.24	4.998	43.6	0.039	2.22	0.006	0.97
T.4.2	0.016	0.19	4.943	44.8	0.037	3.03	0.005	0.97
T.5.1	0.026	0.48	3.470	46.3	0.000	3.07	0.003	0.98
T.5.2	0.025	0.15	4.930	45.7	0.052	3.39	0.004	0.99
T.6.1	0.035	0.12	2.500	41.4	0.000	2.11	0.004	0.96
Median	0.025	0.57	2.500	44.8	0.039	2.11	0.004	0.97
$[Q_1, Q_3]$	$[0.019, 0.033]$	$[0.20, 4.52]$	$[0.000, 4.939]$	$[41.5, 46.5]$	$[0.005, 0.135]$	$[1.23, 2.94]$	$[0.003, 0.007]$	$[0.97, 0.98]$
Abdominal aortic aneurysm								
A.1	0.010	6.16	0.001	41.4	0.249	2.10	0.002	0.92
A.2	0.008	1.54	67.18	41.5	0.104	1.00	0.008	0.96
A.3	0.034	15.1	569.2	41.4	0.270	3.10	0.002	0.90
A.4	0.034	16.5	0.000	43.1	0.266	3.08	0.004	0.95
A.5	0.173	54.5	30.37	48.2	0.316	1.50	0.001	0.92
A.6	0.080	6.03	0.000	39.1	0.252	1.26	0.003	0.87
A.7	0.012	2.08	0.000	41.9	0.151	1.50	0.004	0.94
A.8.1	0.019	2.72	0.000	43.9	0.174	1.20	0.005	0.94
A.8.2	0.026	2.74	119.6	43.2	0.181	1.35	0.004	0.96
Median	0.026	6.03	0.001	41.9	0.249	1.50	0.004	0.93
$[Q_1, Q_3]$	$[0.011, 0.046]$	$[2.56, 15.5]$	$[0.000, 80.20]$	$[41.4, 43.4]$	$[0.169, 0.267]$	$[1.21, 2.34]$	$[0.002, 0.004]$	$[0.91, 0.95]$

Table 2: Median values, interquartile ranges (Q_1 and Q_3) and coefficients of determination R^2 for material and damage parameters fitted to the intact, human thoracic and abdominal aortic aneurysmal tissues.

	μ	k_1	k_2	φ	κ	r_f	m_f	R^2
	[MPa]	[MPa]	[–]	[°]	[–]	[–]	[–]	[–]
Thoracic aorta								
Median	0.017	0.56	16.21	51.0	0.18	1.59	0.008	0.97
$[Q_1, Q_3]$	$[0.014, 0.019]$	$[0.24, 0.94]$	$[5.790, 34.79]$	$[46.8, 53.8]$	$[0.08, 0.28]$	$[1.25, 1.83]$	$[0.004, 0.011]$	$[0.95, 0.98]$
Abdominal aorta								
Median	0.019	5.15	8.64	38.8	0.24	1.10	0.013	0.98
$[Q_1, Q_3]$	$[0.012, 0.042]$	$[2.58, 10.5]$	$[0.00, 32.4]$	$[35.8, 41.1]$	$[0.21, 0.25]$	$[1.00, 1.54]$	$[0.010, 0.019]$	$[0.93, 0.99]$

Table 3: Median values, interquartile ranges (Q_1 and Q_3) and coefficients of determination R^2 for material and damage parameters fitted to the healthy, intact (three-layer composite) human thoracic and abdominal aortic tissues, from Weisbecker et al. (2012).

indicating reduced exponential stiffening.

3.4. Histology

We provide representative histological images for the thoracic aneurysmal sample T.2.1 in Fig. 2 and for the abdominal aneurysmal sample A.8.2 in Fig. 3. The top row (a)-(b) of each figure shows the H&E staining, with cell cores stained dark purple; the middle row (c)-(d) shows the EvG staining, with elastic fibers highlighted black; and the bottom row (e)-(f) shows the PsR staining, with collagenous fibers stained red. We generated images in the left columns with the magnification of the microscope set to $20\times$, while on the right side this is set to $100\times$. Figures in the same columns always show the same section of the samples.

4. Discussion

4.1. Material and damage parameters

In the present work we testes intact, human thoracic and abdominal aortic aneurysmal tissues in uniaxial extension, although biaxial extension testing would better mimic the in vivo loading condition. We dis this because uniaxial extension testing is better suited to higher (supra-physiological) loading and it allowed us to effectively test the relatively small samples available. We overcame the disadvantages of uniaxial testing for our application with a careful experimental protocol and model-fitting procedure (Holzapfel, 2006).

We used a pseudo-elastic constitutive model, introduced by Ogden and Roxburgh (1999), to fit the resulting mechanical data and study damage accumulating in the aortic aneurysmal tissues, causing softening during supra-physiological loading. A big advantage of this model is that we can split the fitting procedure into two parts. First we fitted the primary loading curve described by the elastic strain-energy function. Second, we used the resulting material parameters for the elastic response and fitted the unloading and reloading curves to determine the damage parameters.

Figures 1(a) and (c) provide representative data gathered from mechanical testing as well as the fitted stress-stretch response. The pseudo-elastic constitutive model fits the data from both thoracic and abdominal tissues well. In both cases the material response is clearly anisotropic but the orientation of higher stiffness switches. In these particular samples the thoracic tissue (sample T.2.1) is stiffer in the axial direction while the abdominal tissue (sample A.8.2) is stiffer in the circumferential direction.

Figures 1(b) and (d) provide the corresponding evolution of damage-induced softening, represented by the minimum of the damage variable. The model fits both the discontinuous softening caused by pre-conditioning in the physiological loading range and the softening damage caused during supra-physiological loading. Little is currently known about damage mechanisms within

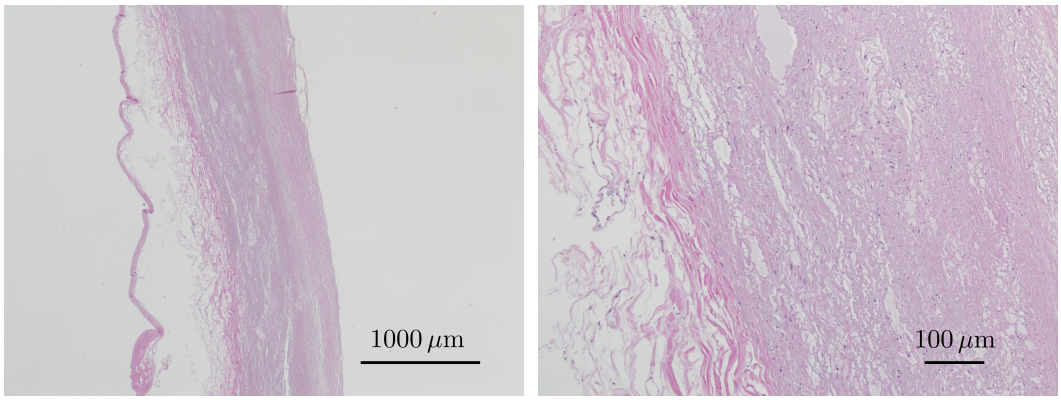

(a) (b)

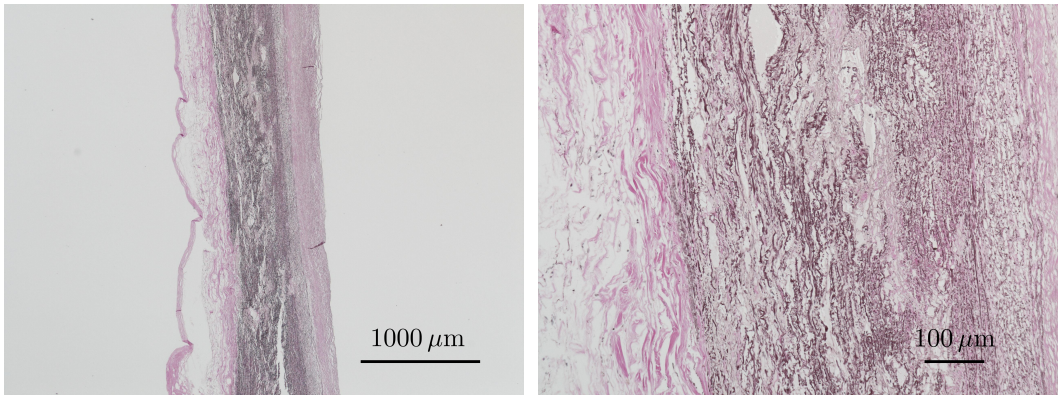

(c) (d)

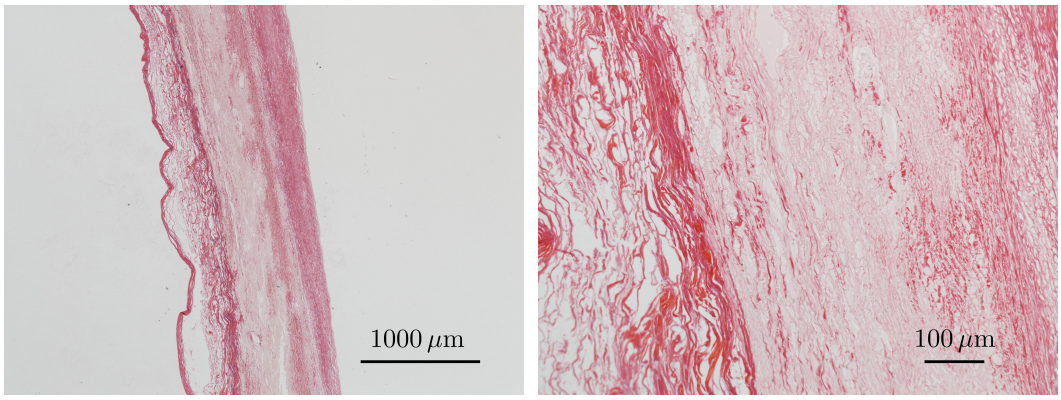

(e) (f)

Figure 2: Representative histological images from the thoracic aneurysmal sample T.2.1: (a)-(b) H&E staining, (c)-(d) EvG staining and (e)-(f) PsR staining, from the entire sample in the left column (scale bar is $1000\,\mu$m) and from a magnified detail in the right column (scale bar is $100\,\mu$m). Figs. 1(a)-(b) show the corresponding mechanical test data, model fit and damage evolution.

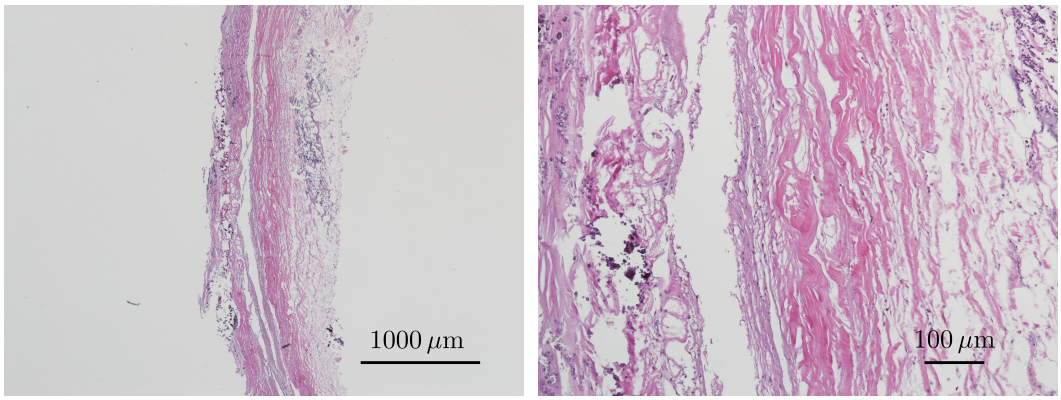

(a) (b)

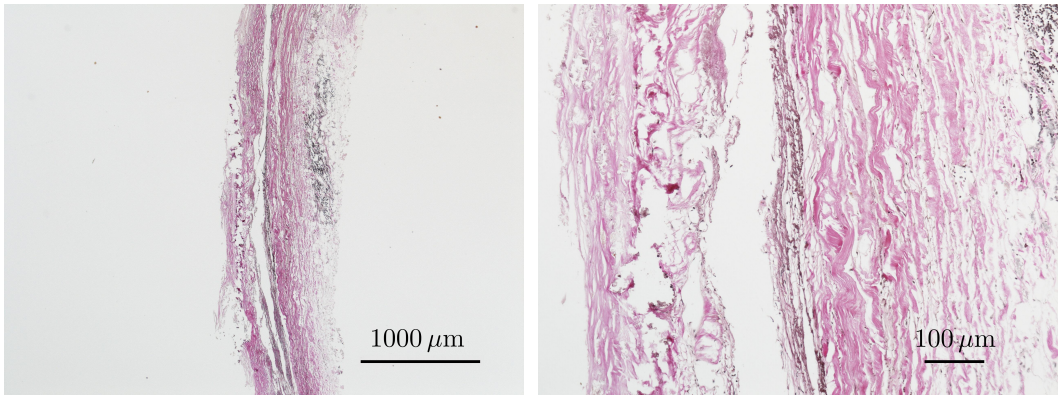

(c) (d)

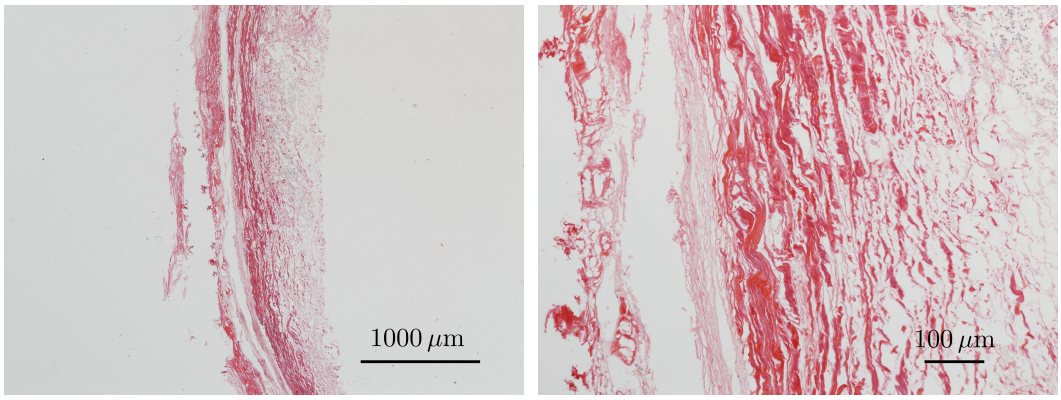

(e) (f)

Figure 3: Representative histological images from the abdominal aneurysmal sample A.8.2: (a)-(b) H&E staining, (c)-(d) EvG staining and (e)-(f) PsR staining, from the entire sample in the left column (scale bar is 1000 μm) and from a magnified detail in the right column (scale bar is 100 μm). Figs. 1(c)-(d) show the corresponding mechanical test data, model fit and damage evolution.

aneurysmal tissues, and whether or not softening that is still in the physiological range, sometimes referred to as preconditioning, should be distinguished from irreversible (inelastic) mechanisms occurring in the tissue structure. Hence, in this study we did not set a threshold value to determine damage initiation. Balzani et al. (2006) calculated the strain-energy accumulated at an internal arterial pressure at $180\,\mathrm{mmHg}$ and defined this as the initial damage state, prohibiting the evolution of softening below this threshold. We were not able to define an objective threshold to distinguish between physiological and non-physiological damage and suggest that more specialized experiments and structural analysis should be performed. This remains a challenging research area because the damage mechanisms which ultimately lead to failure are not well understood.

Table 2 provides median values, interquartile ranges and coefficients of determination for material and damage parameters fitted to the intact, human thoracic and abdominal aortic aneurysmal tissues. Note that nearly all patients had hypertension and hypercholesterolemia (Table A.4), both known risk factors for cardiovascular diseases. Since the fitted model parameters are not normally distributed, we calculated the median values and the corresponding interquartile ranges to represent them properly, with the additional benefit that these values are less sensitive to outliers than the mean values and standard deviations.

The median fiber angle φ for the thoracic aneurysmal tissues is $44.8°$, indicating a nearly isotropic behavior (NB. at $45°$ the circumferential and axial directions appear equally stiff). However, the corresponding interquartile range from $41.5°$ to $46.5°$ shows high variability for the mean fiber orientation, from a circumferentially to an axially fiber-reinforced tissue. Sokolis et al. (2012) tested layer-separated human ascending TAAs and determined that medial and adventitial but not intimal layers were stiffer in the circumferential direction. Similarly, Pham et al. (2013) tested intact ascending aortic aneurysms under biaxial loading and determined that the tissue was stiffer in the circumferential direction. Conversely, Azadani et al. (2013) tested human ascending TAAs and proposed that there is no directional dependency, in accordance to the median value we found.

In contrast, we calculated a median value of $\varphi = 41.9°$, with an interquartile range from $41.4°$ to $43.4°$, for the abdominal aneurysmal tissues. Thus, abdominal aneurysmal tissues show a higher stiffness circumferentially, indicating a primary fiber orientation in this direction, also with less variation. Both Tong et al. (2011) and Vande Geest et al. (2006) reported similar findings. In the future, one could directly measure the fiber directions and the dispersions using methods proposed by, e.g., Schriefl et al. (2012a, 2013), and measurements which could be used to either validate the fitted median fiber angles or improve the accuracy of the fitted model by

using the measured angles of fiber reinforcement as input data (Rodríguez et al., 2009).
Also related to the mechanical response of the collagen fibers, the fitted k_2 values for AAA tissues vary widely from zero (the strain-energy function from (5) is reduced to $\overline{\Psi}^0_{\mathrm{f},i} = k_1(\bar{I}^\star_i - 1)^2/2$, cf. Weisbecker et al., 2012), to relatively high values.
We also found large variations in the thickness within individual samples: the mean value was $2.12\,\mathrm{mm} \pm 0.42$ (mean $\pm$ SD) for the abdominal samples and $1.98\,\mathrm{mm} \pm 0.3$ for the thoracic samples. We also measured substantial variations in the thicknesses within individual samples, e.g., the mean thickness $\pm$ SD of four measured points from abdominal sample A.4 was $2.23\,\mathrm{mm} \pm 0.46$. Raghavan et al. (2006) reported similar variations in intra-sample thicknesses.

4.2. Statistical analysis

We used statistical methods to determine if our model parameters, fitted to data generated from testing of abdominal aortic aneurysmal tissues, correlated significantly with a patient's age, BMI and preoperative aneurysm diameter. Among all combinations tested, only BMI correlated significantly with the model parameters generated from AAA tissues. No correlations were evident among the patient's age and the model parameters, indicating that the age of the aneurysm itself is more important in determining it's mechanical properties, in accordance with Wilson et al. (2012). Additionally, pre-surgical aneurysm diameter has no significant influence on the model parameters. Our result is in accordance with the literature, see, e.g., Vorp (2007), and strengthens the theory that aneurysm diameter is an insufficient measure to recommend surgery. However, the relatively small sample population used in our study could have also caused us to miss significant correlations.
Regarding the significance of differences among the model parameters determined for thoracic versus abdominal aortic aneurysmal tissues, we found such a difference for the parameter k_1 which is larger for the abdominal tissues, indicating that the fibers contribute more to the mechanical response. The parameter κ also differs significantly and is larger for the abdominal tissues, indicating greater larger dispersion.

4.3. Comparison with healthy tissues

We found a significant difference in the parameters μ and k_2 between healthy and diseased abdominal tissues for both thoracic and abdominal samples. Here μ is larger for aneurysmal tissues, indicating a higher stiffness in the low-strain region which could result from replacement of the elastic ground substance in favor of a collagenous network, with increased cross-linking of the collagen fibers (Lindeman et al., 2010). Lindeman et al. (2010) also showed that the collagen fibers of diseased tissues have reduced waviness and thereby appear stiffer at lower

stretches. This is consistent with our findings that the parameter k_2 is lower which means a reduced exponential stiffening of the material occurs relative to healthy tissues. This could be due to a faster fiber recruitment at lower strains in the remodeled collagen network. We also found that the angles of collagen fiber reinforcement φ vary significantly between healthy and diseased tissues. In both cases the aneurysmal tissues become less anisotropic, i.e., closer to $\varphi = 45°$, which is in contrast to Vande Geest et al. (2006) who found anisotropy increased with aneurysm development. Median values for the damage parameter r_{f} are higher for diseased tissues than for healthy tissues. This result indicates that less softening can occur in the diseased tissues. Here again we suggest that more research is necessary to identify the damage mechanism beyond normal physiological loading, because damage is the most likely trigger for remodeling processes, e.g., for restenosis (Timmins et al., 2011), which could also be related to stabilized aneurysms (Vorp, 2007). If significant calcification is evident in the tissue, most likely the softening can be interpreted as non-physiological damage (Mulvihill et al., 2013).

We used a statistical approach to determine the significance of differences among the model parameters fitted to healthy *descending* thoracic tissue samples (from Weisbecker et al., 2012) to those from diseased *ascending* thoracic samples. We know that there are differences in the mechanical properties between healthy ascending and descending thoracic aortic tissues (Roccabianca et al., 2014), but because of the samples available, we assume that we can still capture trends in the changes of model parameters due to aneurysm growth.

Looking at the abdominal samples specifically, the diseased tissues have a median material parameter k_2 which is nearly zero such that the material is related to a quadratic strain-energy function rather than an exponential one. Additionally, the damage parameter m_{f} is significantly lower for abdominal aneurysmal tissues than for healthy tissues, indicating that softening is induced at smaller strains.

Overall our results indicate that aneurysm development has a larger effect on the mechanical response of thoracic aortas than on abdominal aortas. Some remodeling processes, e.g., decrease in elastin, increase in collagen and atherosclerosis, happen in the healthy aorta as part of the normal aging process (Tsamis et al., 2013). Perhaps such effects are more pronounced in the abdominal aorta, effects which would change the initial condition of the tissue for disease initiation (Wilson et al., 2012), i.e. a more remodeled initial tissue would appear to change less in disease.

4.4. Histology

The main goal of our histological investigations was to better understand the morphology of the aneurysms, and thus to better interpret our model parameters (and changes in these). Results

indicate a significant difference between the TAA and the AAA tissues.
The TAA samples appeared overall more intact. Figures 2 and 3 show similar signs of calcification and collagen remodeling, but these appear more severe in the AAA samples. Additionally, the content of both elastin (shown in Fig. 2(d) as black fibers) and smooth muscle cells (shown as cell cores in Fig. 2(b)) was higher in the thoracic samples.
In contrast, the AAA samples were highly remodeled, where the number of both elastic fibers and smooth muscle cells was drastically reduced and largely replaced by collagen fiber bundles, as shown in Fig. 3. In Fig. 3(b) the absence of smooth muscle cells is visible. In Fig. 3(c) the absence of elastin is visible over large areas of the sample, elastin which is replaced by collagen, as show in Fig. 3(e). Signs of atherosclerosis presented as high calcification in all the AAA samples, shown as crystalline structures in the histological cuts, e.g., on the left side in Fig. 3(d). In some cases, dramatic wall defects were also present.
Differences in the model parameters related to these structural differences. The collagen network which replaces softer elastin matrix corresponds to an increased mechanical influence of collagen, represented by a relatively higher value of the parameter k_1.
In all AAA samples, highly concentrated cell clusters, shown as accumulations of black dots on the right side of the tissue sample in Fig. 3(a), indicate the presence of inflammation. Such concentrated cell clusters were less common in the TAA samples and if present, not as distinct. Inflammation could play a key role in the development and growth of aneurysms, especially for AAA, according to Thompson (2005) and Shimizu et al. (2006).

4.5. Applications and shortcomings

Due to large patient variability, 'one criterion for all' approaches to estimate the rupture risk of aneurysms are unlikely to be accurate when applied to individuals. The main goal of this study was to obtain material parameters for abdominal and thoracic aortic aneurysmal tissues to facilitate FE analysis. Future methods for risk estimation of aneurysm rupture should tend toward patient-specificity, e.g., FE simulations calibrated using medical images for building geometry, and constitutive models and fitted parameters such as those provided here. In light of the degeneration of active cells, the mechanical properties of highly remodeled aortic aneurysmal tissues might be fully characterized with passive testing alone.
Regarding our experiments, to our best knowledge no information about the influence of storage at -20°C on the mechanical properties of human aneurysmal tissues is available. Adham et al. (1996) performed mechanical experiments with human tissue stored at -135°C and concluded that cryopreservation did not alter the mechanical characteristics of human descending

thoracic aorta. Venkatasubramanian et al. (2006) investigated the changing mechanical behavior of femoral arteries from pigs due to freezing at -20°C and -80°C and concluded that major changes are only evident in the low-strain region of the mechanical response. In contrast, Chow and Zhang (2011) performed biaxial mechanical experiments on bovine thoracic aortas that had been stored at common storage temperatures (4°C, -20°C, or -80°C) for three different time points (48 hours, 1 week, or 3 weeks). For a storage at -20°C the authors found no significant change in the low-strain regime but a significant shift in the high-strain regime of the mechanical response. Chow and Zhang (2011) concluded that there are changes within the tissue most likely due to intracellular ice formation.

Due to large variability in the fitted model parameters, naive use of the median parameters could lead to serious errors in FE simulations aimed at estimating stresses or aneurysm rupture risk. With improving imaging techniques, such as, e.g., optical coherence tomography (van Soest et al., 2010), intravascular ultrasound (Suzuki et al., 2008) or B-mode ultrasound (de Groot et al., 2008), in vivo estimation of the tissue state might allow an accurate implementation of inhomogeneous material properties and therefore the range of material parameters might be of greater interest than median values. Kaladji et al. (2013) implemented a simplified attempt in this direction by varying the Young's modulus of arteries, in an FE simulation of endovascular insertion for aortic aneurysm repair, depending on an image-based estimate of the calcification level along the path of the guide wire. The determination and correct use of appropriate material parameters for simulations in soft tissue biomechanics, e.g., those of AAAs and TAAs, remains a major challenge in biomechanics (Miller and Lu, 2013).

In this study we neglected the active mechanical response of smooth muscle cells within the aortic tissues. In the highly remodeled AAA tissues this simplification should be acceptable. In the TAA tissues, where the muscle cells appeared largely intact, this simplification may be problematic. We would require more sophisticated constitutive models to account for the active response of the muscle cells, where biochemical processes are additionally considered, see, e.g., Murtada et al. (2012); Murtada and Holzapfel (2014).

Finally, simulations based on the data provided here can only account for a single point in time, no long-term behavior and biological responses can be predicted with our fitted constitutive model. To simulate the time evolution of an aneurysm growth models, e.g., by Satha et al. (2014) or remodeling models, e.g., by Hadi et al. (2012) for collagen networks, must be implemented. Nevertheless, for predicting failure and quantifying damage immediately after supra-physiological loading, e.g., balloon angioplasty, the model provided here suffices.

Acknowledgments

We gratefully acknowledge the financial support of the European Commission under the 7^{th} Framework Programme in the scope of the project SCATh – Smart Catheterization, Grant Agreement Number 248782.

Appendix A. Additional Patient-Specific Data

Patient #	Hypertension –	Diabetic –	hypercholesterolemia –	Smoke –	Drink (W/B/C)/week	Caffeine cups/day	Sport hours/week
Thoracic aortic aneurysm							
T.1	1	1	1	0	0/0/0	2	0
T.2	3	0	2	0	2/0/0	2	0
T.3	1	0	0	0	0/0/0	0	0
T.4	2	0	2	0	NA	NA	NA
T.5	0	0	0	0	NA	NA	NA
Abdominal aortic aneurysm							
A.1	1	1	1	NA	0/7/0	5	0
A.2	1	0	1	0	2/2/0	5	0
A.3	1	0	1	0	0/3/0	5	0
A.4	1	1	1	1	2/0/0	5	0
A.5	1	0	1	2	0/0/0	5	0
A.6	1	0	1	0	0/0/0	5	2
A.7	1	0	1	1	3/2/0	1	5
A.8	1	0	1	0	NA	5	0

Table A.4: Patient-specific data on the medical background and lifestyle: in columns 'Hypertension', 'Diabetic' and 'hypercholesterolemia' 0 indicates no diagnosis, 1 or higher indicates that the disease was detected and treated with the corresponding number of medications. In column 'Smoke' 0 indicates the patient never smoked or stopped more than 10 years ago, 1 indicates stopped in the last 10 years and 2 indicates current smoking of less than one pack per day. In column 'Drink' W/B/C indicates number of glasses of wine, beer and cocktails per week, respectively. The columns 'Caffeine' and 'Sport' indicate the number of cups of caffeinated beverages per day and hours of sport per week, respectively. 'NA' = data not available.

References

Adham, M., Gournier, J. P., Favre, J. P., De La Roche, E., Ducerf, C., Baulieux, J., Barral, X., Pouyet, M., 1996. Mechanical characteristics of fresh and frozen human descending thoracic aorta. J. Surg. Res. 64, 32–34.

Azadani, A. N., Chitsaz, S., Mannion, A., Mookhoek, A., Wisneski, A., Guccione, J. M., Hope, J. M., Ge, M. D., Tseng, E. E., 2013. Biomechanical properties of human ascending thoracic aortic aneurysms. Ann. Thorac Surg. 96, 50–58.

Badel, P., Avril, S., Sutton, M. A., Lessner, S. M., 2014. Numerical simulation of arterial dissection during balloon angioplasty of atherosclerotic coronary arteries. J. Biomech. 47, 878–889.

Balakhovsky, K., Jabareen, M., Volokh, K. Y., 2014. Modeling rupture of growing aneurysms. J. Biomech. 47, 653–658.

Balzani, D., Brinkhues, S., Holzapfel, G. A., 2012. Constitutive framework for the modeling of damage in collagenous soft tissues with application to arterial walls. Comput. Meth. Appl. Mech. Eng. 213-216, 139–151.

Balzani, D., Schröder, J., Gross, D., 2006. Simulation of discontinuous damage incorporating residual stresses in circumferentially overstretched atherosclerotic arteries. Acta Biomater. 2, 609–618.

Chai, C. K., Akyildiz, A. C., Speelman, L., Gijsen, F. J., Oomens, C. W., van Sambeek, M. R., van der Lugt, A., Baaijens, F. P., 2013. Local axial compressive mechanical properties of human carotid atherosclerotic plaques – characterisation by indentation test and inverse finite element analysis. J. Biomech. 46, 1759–1766.

Chow, M. J., Zhang, Y., 2011. Changes in the mechanical and biochemical properties of aortic tissue due to cold storage. J. Surg. Res. 171, 434–442.

de Groot, E., van Leuven, S. I., Duivenvoorden, R., Meuwese, M. C., Akdim, F., Bots, M. L., Kastelein, J. J., 2008. Measurement of carotid intima-media thickness to assess progression and regression of atherosclerosis. Nat. Clin. Pract. Cardiovasc. Med. 5, 280–288.

Famaey, N., Sommer, G., Vander Sloten, J., Holzapfel, G. A., 2012. Arterial clamping: Finite element simulation and in vivo validation. J. Mech. Behav. Biomed. Mater. 12, 107–118.

Gasser, T. C., 2011. An irreversible constitutive model for fibrous soft biological tissue: a 3-D microfiber approach with demonstrative application to abdominal aortic aneurysms. Acta Biomater. 7, 2457–2466.

Gasser, T. C., Ogden, R. W., Holzapfel, G. A., 2006. Hyperelastic modelling of arterial layers with distributed collagen fibre orientations. J. R. Soc. Interface 3, 15–35.

Hadi, M. F., Sander, E. A., Ruberti, J. W., Barocas, V. H., 2012. Simulated remodeling of loaded collagen networks via strain-dependent enzymatic degradation and constant-rate fiber growth. Mech. Mat. 44, 72–82.

Holzapfel, G. A., 2006. Determination of material models for arterial walls from uniaxial extension tests and histological structure. J. Theor. Biol. 238, 290–302.

Holzapfel, G. A., Gasser, T. C., Ogden, R. W., 2000. A new constitutive framework for arterial wall mechanics and a comparative study of material models. J. Elasticity 61, 1–48.

Humphrey, J. D., Holzapfel, G. A., 2012. Mechanics, mechanobiology, and modeling of human abdominal aorta and aneurysms. J. Biomech. 45, 805–814.

Iannaccone, F., Debusschere, N., De Bock, S., De Beule, M., Van Loo, D., Vermassen, F., Segers, P., Verhegghe, B., 2014. The influence of vascular anatomy on carotid artery stenting: A parametric study for damage assessment. J. Biomech. 47, 890–898.

Kaladji, A., Dumenil, A., Castro, M., Cardon, A., Becquemin, J. P., Bou-Saïd, B., Lucas, A., Haigron, P., 2013. Prediction of deformations during endovascular aortic aneurysm repair using finite element simulation. Comput. Med. Imag. Grap. 37, 142–149.

Kitagawa, A., Mastracci, T. M., von Allmen, R., Powell, J. T., 2013. The role of diameter versus volume as the best prognostic measurement of abdominal aortic aneurysms. J. Vasc. Surg. 58, 258–265.

Kniemeyer, H. W., Kessler, T., Reber, P. U., Ris, H. B., Hakki, H., Widmer, M. K., 2000. Treatment of ruptured abdominal aortic aneurysm, a permanent challenge or a waste of resources? prediction of outcome using a multi-organ-dysfunction score. Eur. J. Vasc. Endovasc. Surg. 19, 190–196.

Lederle, F. A., Wilson, S. E., Johnson, G. R., Reinke, D. B., Littooy, F. N., Acher, C. W., Ballard, D. J., Messina, L. M., Gordon, I. L., Chute, E. P., Krupski, W. C., Busuttil, S. J., Barone,

G. W., Sparks, S., Graham, L. M., Rapp, J. H., Makaroun, M. S., Moneta, G. L., Cambria, R. A., Makhoul, R. G., Eton, D., Ansel, H. J., Freischlag, J. A., Bandyk, D., Aneurysm Detection and Management Veterans Affairs Cooperative Study Group, 2002. Immediate repair compared with surveillance of small abdominal aortic aneurysms. N. Engl. J. Med. 346, 1437–1444.

Lindeman, J. H., Ashcroft, B. A., Beenakker, J. W., van Es, M., Koekkoek, N. B., Prins, F. A., Tielemans, J. F., Abdul-Hussien, H., Bank, R. A., Oosterkamp, T. H., 2010. Distinct defects in collagen microarchitecture underlie vessel-wall failure in advanced abdominal aneurysms and aneurysms in Marfan syndrome. Proc. Natl. Acad. Sci. USA 107, 862–865.

Martin, C., Sun, W., Pham, T., Elefteriades, J., 2013. Predictive biomechanical analysis of ascending aortic aneurysm rupture potential. Acta Biomater. 9, 9392–9400.

Miller, K., Lu, J., 2013. On the prospect of patient-specific biomechanics without patient-specific properties of tissues. J. Mech. Behav. Biomed. Mater. 27, 154–166.

Mortier, P., Holzapfel, G. A., De Beule, M., Van Loo, D., Taeymans, Y., Segers, P., Verdonck, P., Verhegghe, B., 2010. A novel simulation strategy for stent insertion and deployment in curved coronary bifurcations: comparison of three drug-eluting stents. Ann. Biomed. Eng. 38, 88–99.

Mulvihill, J. J., Cunnane, E. M., McHugh, S. M., Kavanagh, E. G., Walsh, S. R., Walsh, M. T., 2013. Mechanical, biological and structural characterization of in vitro ruptured human carotid plaque tissue. Acta Biomater. 9, 9027–9035.

Murtada, S., Holzapfel, G. A., 2014. Investigating the role of smooth muscle cells in large elastic arteries: a finite element analysis. J. Theor. Biol., in press.

Murtada, S. C., Arner, A., Holzapfel, G. A., 2012. Experiments and mechanochemical modeling of smooth muscle contraction: significance of filament overlap. J. Theor. Biol. 297, 176–186.

Nichols, M., Townsend, N., Luengo-Fernandez, R., Leal, J., Gray, A., Scarborough, P., Rayner, M., 2012. European Cardiovascular Disease Statistics 2012. Brussels: European Heart Network, Sophia Antipolis: European Society of Cardiology.

Ogden, R. W., Roxburgh, D. G., 1999. A pseudo-elastic model for the Mullins effect in filled rubber. Proc. R. Soc. Lond. A 455, 2861–2877.

Ogden, R. W., Saccomandi, G., Sgura, I., 2004. Fitting hyperelastic models to experimental data. Comput. Mech. 34, 484–502.

Peña, E., Peña, J. A., Doblaré, M., 2009. On the Mullins effect and hysteresis of fibered biological materials: A comparison between continuous and discontinuous damage models. Int. J. Solids Structures 46, 1727–1735.

Pham, T., Martin, C., Elefteriades, J., Sun, W., 2013. Biomechanical characterization of ascending aortic aneurysm with concomitant bicuspid aortic valve and bovine aortic arch. Acta Biomater. 9, 7927–7936.

Raghavan, M. L., Kratzberg, J., Castro de Tolosa, E. M., Hanaoka, M. M., Walker, P., da Silva, E. S., 2006. Regional distribution of wall thickness and failure properties of human abdominal aortic aneurysm. J. Biomech. 39, 3010–3016.

Raut, S. S., Chandra, S., Shum, J., Finol, E. A., 2013. The role of geometric and biomechanical factors in abdominal aortic aneurysm rupture risk assessment. Ann. Biomed. Eng. 41, 1459–1477.

Rickaby, S. R., Scott, N. H., 2013. A model for the Mullins effect during multicyclic equibiaxial loading. Acta Mech. 224, 1887–1900.

Roccabianca, S., Figueroa, C. A., Tellides, G., Humphrey, J. D., 2014. Quantification of regional differences in aortic stiffness in the aging human. J. Mech. Behav. Biomed. Mater. 29, 618–634.

Rodríguez, J. F., Cacho, F., Bea, J. A., Doblaré, M., 2006. A stochastic-structurally based three dimensional finite-strain damage model for fibrous soft tissue. J. Mech. Phys. Solids 54, 864–886.

Rodríguez, J. F., Martufi, G., Doblaré, M., Finol, E. A., 2009. The effect of material model formulation in the stress analysis of abdominal aortic aneurysms. Ann. Biomed. Eng. 37, 2218–2221.

Rodríguez, J. F., Ruiz, C., Doblaré, M., Holzapfel, G. A., 2008. Mechanical stresses in abdominal aortic aneurysms: influence of diameter, asymmetry and material anisotropy. J. Biomech. Eng. 130, 021023–1–10.

Romo, A., Badel, P., Duprey, A., Favre, J. P., Avril, S., 2014. In vitro analysis of localized aneurysm rupture. J. Biomech. 47, 607–616.

Satha, G., Lindström, S. B., Klarbring, A., 2014. A goal function approach to remodeling of arteries uncovers mechanisms for growth instability. Biomech. Model. Mechanobiol.[Epub ahead of print].

Schmidt, T., Balzani, D., Holzapfel, G. A., 2014. Statistical approach for a continuum description of damage evolution in soft collagenous tissues. Comput. Meth. Appl. Mech. Eng. 278, 41–61.

Schriefl, A. J., Reinisch, A. J., Sankaran, S., Pierce, D. M., Holzapfel, G. A., 2012a. Quantitative assessment of collagen fiber orientations from 2D images of soft biological tissues. J. R. Soc. Interface 9, 3081–3093.

Schriefl, A. J., Wolinski, H., Regitnig, P., Kohlwein, S. D., Holzapfel, G. A., 2013. An automated approach for 3D quantification of fibrillar structures in optically cleared soft biological tissues. J. R. Soc. Interface 10, 20120760.

Schriefl, A. J., Zeindlinger, G., Pierce, D. M., Regitnig, P., Holzapfel, G. A., 2012b. Determination of the layer-specific distributed collagen fiber orientations in human thoracic and abdominal aortas and common iliac arteries. J. R. Soc. Interface 9, 1275–1286.

Shimizu, K., Mitchell, R. N., Libby, P., 2006. Inflammation and cellular immune responses in abdominal aortic aneurysms. Arterioscler. Thromb. Vasc. Biol. 26, 987–994.

Sokolis, D. P., Kritharis, E. P., Iliopoulos, D. C., 2012. Effect of layer heterogeneity on the biomechanical properties of ascending thoracic aortic aneurysms. Med. Biol. Eng. Comput. 50, 1227–1237.

Suzuki, Y., Ikeno, F., Koizumi, T., Tio, F., Yeung, A. C., Yock, P. G., Fitzgerald, P. J., Fearon, W. F., 2008. In vivo comparison between optical coherence tomography and intravascular ultrasound for detecting small degrees of in-stent neointima after stent implantation. JACC Cardiovasc. Interv. 1, 168–173.

Thompson, R. W., 2005. Aneurysm treatments expand. Nat. Med. 11, 1279–1281.

Timmins, L. H., Miller, M. W., Clubb Jr, F. J., Moore Jr, J. E., 2011. Increased artery wall stress post-stenting leads to greater intimal thickening. Lab. Invest. 91, 955–967.

Tong, J., Cohnert, T., Regitnig, P., Holzapfel, G. A., 2011. Effects of age on the elastic properties of the intraluminal thrombus and the thrombus-covered wall in abdominal aortic aneurysms: biaxial extension behavior and material modeling. Eur. J. Vasc. Endovasc. Surg. 42, 207–219.

Tong, J., Cohnert, T., Regitnig, P., Kohlbacher, J., Birner-Gruenberger, R., Schriefl, A. J., Sommer, G., Holzapfel, G. A., 2014. Variations of dissection properties and mass fractions with thrombus age in human abdominal aortic aneurysms. J. Biomech. 47, 14–23.

Tsamis, A., Krawiec, J. T., Vorp, D. A., 2013. Elastin and collagen fibre microstructure of the human aorta in ageing and disease: a review. J. R. Soc. Interface 10, 20121004.

van Soest, G., Goderie, T., Regar, E., Koljenović, S., van Leenders, G. L., Gonzalo, N., van Noorden, S., Okamura, T., Bouma, B. E., Tearney, G. J., Oosterhuis, J. W., Serruys, P. W., van der Steen, A. F., 2010. Atherosclerotic tissue characterization in vivo by optical coherence tomography attenuation imaging. J. Biomed. Opt. 15, 011105–9.

Vande Geest, J. P., Sacks, M. S., Vorp, D. A., 2006. The effects of aneurysm on the biaxial mechanical behavior of human abdominal aorta. J. Biomech. 39, 1324–1334.

Vande Geest, J. P., Schmidt, D. E., Sacks, M. S., Vorp, D. A., 2008. The effect of anisotropy on the stress analyses of patient-specific abdominal aortic aneurysms. Ann. Biomed. Eng. 36, 921–932.

Venkatasubramanian, R. T., Grassl, E. D., Barocas, V. H., Lafontaine, D., Bischof, J. C., 2006. Effects of freezing and cryopreservation on the mechanical properties of arteries. Ann. Biomed. Eng. 34, 823–832.

Volokh, K. Y., Vorp, D. A., 2008. A model of growth and rupture of abdominal aortic aneurysm. J. Biomech. 41, 1015–1021.

Vorp, D. A., 2007. Biomechanics of abdominal aortic aneurysm. J. Biomech. 40, 1887–1902.

Weisbecker, H., Pierce, D. M., Regitnig, P., Holzapfel, G. A., 2012. Layer-specific damage experiments and modeling of human thoracic and abdominal aortas with non-atherosclerotic intimal thickening. J. Mech. Behav. Biomed. Mater. 12, 93–106.

Wilson, J. S., Baek, S., Humphrey, J. D., 2012. Importance of initial aortic properties on the evolving regional anisotropy, stiffness and wall thickness of human abdominal aortic aneurysms. J. R. Soc. Interface 9, 2047–2058.

Wu, M., Rementer, C., Giachelli, C. M., 2013. Vascular calcification: An update on mechanisms and challenges in treatment. Calcif. Tissue Int. 93, 365–373.